Improved Vernier effect scheme based on a single interferometer with unique wavelength and compact structure

Yunqing Guan, Yingbin Feng, Yuanyang Chen, Lina Ma, Feng Xia, Matthias Fabian, Dongsheng Wu, Hongwei Gao, Tong Sun, and Kenneth T. V. Grattan

***Abstract*—The optical Vernier effect scheme has proven to be a powerful tool for significantly enhancing the sensitivity of the interferometric sensors by combining two interferometers, provided that the Free Spectral Range (FSR) of each interferometer closely matches that of the other. However, the fabrication of a reference cell that precisely aligns with the sensing interferometer to meet the Vernier condition can be challenging. In this paper, we propose a novel Vernier effect scheme consisting of only one interferometer. The single interferometer functions as both the sensing interferometer and reference interferometer, where the reference spectrum can be achieved by inverting the sensing spectrum along its wavelength axis. By combining the sensing spectrum and reference spectrum, the resulting Vernier envelope features a unique wavelength, breaking the periodicity seen in the conventional envelope. The sensitivity enhancement principle of the proposed Vernier effect has been theoretically investigated and its effectiveness has been validated experimentally in a temperature measurement. This study offers the advantages of simplicity and cost-effectiveness, with promising potential to improve the performance of Vernier effect–based sensors. It paves the way for achieving higher sensitivity with a more compact sensor configuration, which is highly beneficial for practical sensing applications.**

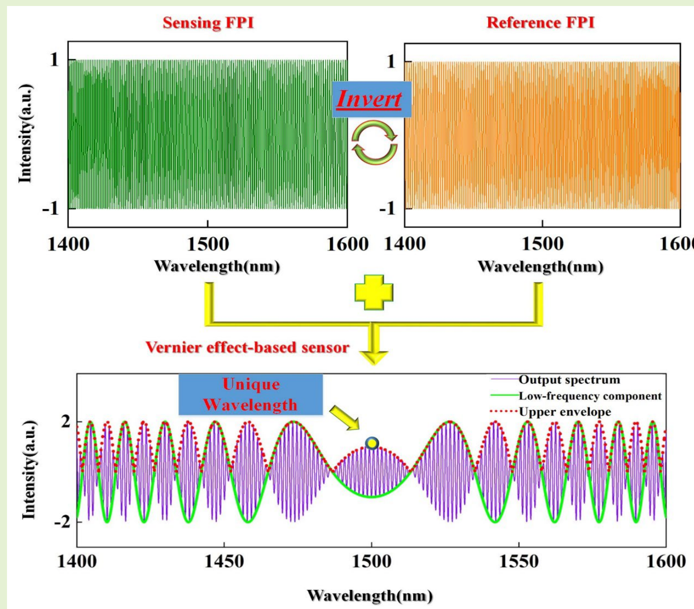

***Index Terms*—Vernier effect, inverted spectrum, unique wavelength, sensitivity enhancement, compact sensor configuration.**

I. INTRODUCTION

THE optical Vernier effect has been widely adopted and studied in various fields, by virtue of its great sensitivity enhancement compared with that of a single interferometric sensor [1], [2], [3]. Typically, a Vernier effect scheme includes two optical interferometers: one is used as a sensing element that reacts to the measurand, while the other acts as a reference cell and is immune to any environmental factor [4], [5]. A substantial Vernier envelope can be extracted through the output spectrum cascaded or paralleled by the two

This work was supported by the basic scientific research project of Liaoning Provincial Department of Education (Grant Number: LJ212410144058), the open fund for the State Key Laboratory of Robotics (Grant Number: 2023O03), the special fund for basic Scientific Research of Colleges and Universities of Liaoning Province (Grant Number: SYLUGXXZ07), the Liaoning Provincial Department of Education's Higher Education Institutions Scientific Research Project (Grant Number: JYTZD2023006), Heilongjiang Province Ecological Environment Protection Scientific Research Project of China (Grant Number: HST2022S006), and the National Natural Science Foundation of China (Grant Number: 62103290).

Yunqing Guan, Yingbin Feng and Dongsheng Wu are with the School of Automation and Electrical Engineering, Shenyang Ligong University, Shenyang 110159, China. (email: yunqingguan@sylu.edu.cn; sylg_fyb@sylu.edu.cn; wuds@sylu.edu.cn). Hongwei Gao is with the Institute of International Engineering, Shenyang LiGong University, Shenyang 110159, China. (email: ghw1978@sylu.edu.cn). Matthias Fabian and Tong Sun are with the School of Mathematics, Computer Science and Engineering, City, University of London, London EC1V 0HB, U.K.(e-mail: matthias.fabian.1@city.ac.uk; t.sun@city.ac.uk). Yuanyang Chen is with the Intellectual Property Research Institute of Xiamen University, and also with the Company of Zhi Ping Zhi Jian (Xiamen) Appraisal Research Institute Limited, Xiamen 361000, China. (email: cyy@fine-pat.com). Lina Ma is with the School of Environment, Harbin Institute of Technology, Harbin 150001, China (email: malina@hit.edu.cn). Feng Xia is with the College of Information Science and Engineering, Shenyang University of Technology, Shenyang, 110870, China. (email: xiafeng@sut.edu.cn). Kenneth T. V. Grattan is with the City Graduate School, City, University of London, London EC1V 0HB, U.K., and also with the School of Mathematics, Computer Science and Engineering, City, University of London, London EC1V 0HB, U.K.(e-mail: k.t.v.grattan@city.ac.uk). Corresponding authors: Yunqing Guan, Hongwei Gao.

interferometers when the Vernier condition is satisfied, i.e. the reference FSR closely matches the sensing one. The variation of the measurand can be detected by the response of the Vernier envelope to improve sensitivity.

Despite its enhanced sensitivity, the traditional Vernier effect scheme faces several inherent challenges. A key issue concerns the sensitivity enhancement factor of the Vernier effect-based sensor, commonly denoted as M [6], [7]. The value of M is determined by the FSR proximity of the two interferometers, which limits its application range. To fabricate the two interferometers with similar FSRs requires additional technologies such as chemical etching [8], [9], electronic discharge [10], [11], or laser machining [12], [13], which brings a bulky and complex manufacturing process with high costs. In addition, maintaining stability in the reference interferometer throughout the detection process is essential. Otherwise, the output spectrum may respond randomly to the measurand, rendering the measurement unreliable.

The harmonic Vernier effect provides an effective method to increase the value of M and overcomes the limitations of the conventional Vernier effect [14], [15], [16]. This is achieved by extending the optical path length of one interferometer to be an integral multiple of the other, with a small deviation. However, as the harmonic order increases, the contrast of the generated Vernier envelope diminishes, and the signal noise reduces the modulation visibility [17]. Besides, the stability concern of the reference interferometer remains. An alternative approach is the virtual Vernier effect, where an artificial reference spectrum is digitally constructed to match the sensing spectrum [18], [19], [20]. This allows for the design of an optimal virtual reference cavity with a series of theoretical calculations, to maximize the sensitivity while keeping the reference cell stable during the measurement process. This method offers the advantages of low cost and precise FSR control, yet the complex derivation and construction of the optimal digital reference cell makes it less suitable for real-time monitoring applications.

Considering that the conventional Vernier effect relies on the superposition of two interferometric spectra with similar FSRs. Since the FSR of a single interferometric spectrum varies slightly with the wavelength, inverting the spectrum along its wavelength axis creates a new spectrum with a similar FSR at different wavelengths compared with the original spectrum, satisfying the Vernier condition. In this work, we propose this novel Vernier effect scheme that features a unique wavelength in the output spectrum and a compact configuration, providing obvious advantages in simplicity and cost-effectiveness. Only one interferometric sensor is involved, serving as both the sensing cell and the reference cell. The effectiveness of the proposed approach is demonstrated through an experimental case, achieving a temperature sensitivity of 2.75 nm/°C, which is 19 times greater than that of a single sensor.

II. Theoretical Analysis

A. Sensitivity Enhancement Principle Of The Novel Vernier Effect Scheme

The proposed Vernier effect scheme incorporates only one interferometer, which functions as both the sensing Fabry-Perot Interferometer (FPI) and the reference FPI. When it operates as the sensing interferometer, the AC component of its output spectrum intensity (denoted as I_s) and its FSR (denoted as FSR_s), can be expressed as [21], [22]:

$$I_s = cos\frac{4\pi nL_s}{\lambda}, FSR_s = \frac{\lambda_1\lambda_2}{2nL_s} \tag{1}$$

Where n is the refractive index of the cavity medium, and L_s is the cavity length of the sensing FPI. λ_1 and λ_2 represent two adjacent peak or dip wavelengths in the sensing spectrum. The spectrum of the reference FPI can be generated by overturning the sensing spectrum along its wavelength axis. To achieve this, the central wavelength of the spectrum, denoted as λ_0, needs to be determined and is given by:

$$\lambda_0 = \frac{\lambda_{max} + \lambda_{min}}{2} \tag{2}$$

Where λ_{max} and λ_{min} are the maximum wavelength and the minimum wavelength within the wavelength range of the spectrum. The sensing spectrum is then overturned along the wavelength axis, using λ_0 as the symmetry center, to obtain the reference spectrum. The intensity of the reference spectrum, represented by I_r, is given by:

$$I_r = cos\frac{4\pi nL_s}{2\lambda_0 - \lambda} \tag{3}$$

The theoretical model of the proposed Vernier effect scheme can be analogized as two FPIs connected in parallel, as assumed in our analysis. The intensity of the combined output spectrum, denoted as I_{sum}, can be written as:

$$\begin{aligned} I_{sum} &= I_s + I_r \\ &= 2cos\left(\frac{2\pi nL_s}{\lambda} - \frac{2\pi nL_s}{2\lambda_0 - \lambda}\right)cos\left(\frac{2\pi nL_s}{\lambda} + \frac{2\pi nL_s}{2\lambda_0 - \lambda}\right) \end{aligned} \tag{4}$$

The generation of the I_{sum} vs. λ curve is illustrated in Fig. 1, covering the wavelength range from 1400 nm to 1600 nm. Fig. 1(a) shows the sensing spectrum, while Fig. 1(b) displays the reference spectrum. In Fig. 1(c), the green curve represents the low-frequency component of the total output spectrum, which is expressed as $2cos(\frac{2\pi nL_s}{\lambda} + \frac{2\pi nL_s}{2\lambda_0 - \lambda})$. A substantial Vernier envelope is generated by fitting the peaks of the high-frequency fringes, illustrated by the red dots. Notably, a unique wavelength appears in the simulated spectrum, marked by the red arrow, which breaks the periodicity of the conventional Vernier envelope. This phenomenon facilitates the use of wavelength tracking methods in long-term measurement applications.

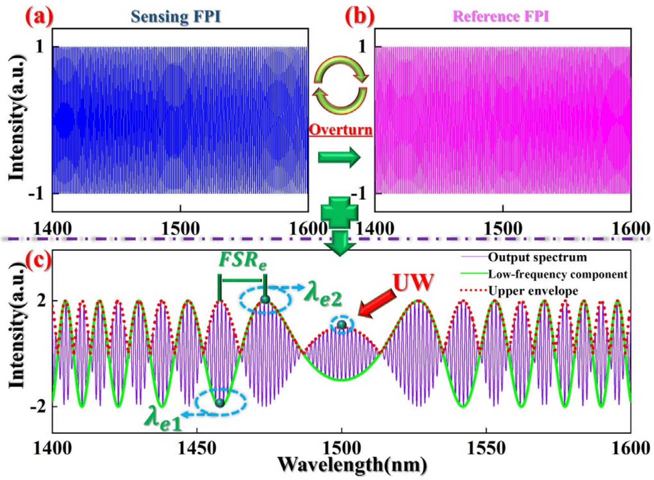

Fig.1. (a) Simulated sensing spectrum. (b) Simulated reference spectrum. (c) Simulated output spectrum of the proposed scheme (Simulation parameters: $L_s = 800$ μm, n = 1; UW: Unique Wavelength).

As shown in Fig.1(c), λ_{e1} and λ_{e2} are the adjacent dip and peak wavelengths in the low-frequency component. Meanwhile, they represent the two adjacent peak wavelengths of the upper Vernier envelope. The phases of λ_{e1} and λ_{e2}, denoted as $\varphi_{\lambda_{e1}}$ and $\varphi_{\lambda_{e2}}$, satisfy:

$$\varphi_{\lambda_{e1}} - \varphi_{\lambda_{e2}} = \pi = \left| \frac{2\pi n L_s}{\lambda_{e1}} + \frac{2\pi n L_s}{2\lambda_0 - \lambda_{e1}} - \frac{2\pi n L_s}{\lambda_{e2}} - \frac{2\pi n L_s}{2\lambda_0 - \lambda_{e2}} \right| \tag{5}$$

On this basis, the FSR of the Vernier envelope, denoted as FSR_e, can be deduced as:

$$FSR_e = \left| \frac{1}{2nL_s \left(\frac{1}{(2\lambda_0 - \lambda_{e1})(2\lambda_0 - \lambda_{e2})} + \frac{1}{\lambda_{e1}\lambda_{e2}} \right)} \right| \tag{6}$$

For the interferometric sensors, the sensitivity enhancement of the Vernier effect-based sensor, compared with the single sensing interferometer, can be denoted by the factor M [23], [24]. In the proposed Vernier effect scheme, M can be further deduced as:

$$M = \frac{FSR_e}{FSR_s} = \left| \frac{1}{1 - \frac{1}{\left(\frac{2\lambda_0}{\lambda_{e1}} - 1\right)\left(\frac{2\lambda_0}{\lambda_{e2}} - 1\right)}} \right| \tag{7}$$

According to equation (7), when λ_{e1} and λ_{e2} approach λ_0, the value of M tends to infinity. Therefore, the peak or dip wavelength in the Vernier envelope nearest to λ_0 can be selected as the monitoring wavelength. The proposed scheme enables the generation of a Vernier effect using only a single interferometer configuration, allowing for high-sensitivity measurements.

B. Validation Of Simulation Results

To provide a clearer demonstration, a simulation was conducted using the change in the cavity length of the sensing interferometer as an example. The simulation parameters are the same as those in Fig. 1. When L_s changes by 0.1 μm, 0.2 μm, 0.3 μm, and 0.4 μm, respectively, the spectra and the response of the sensing interferometer are shown in Fig. 2(a) and Fig. 2(b).

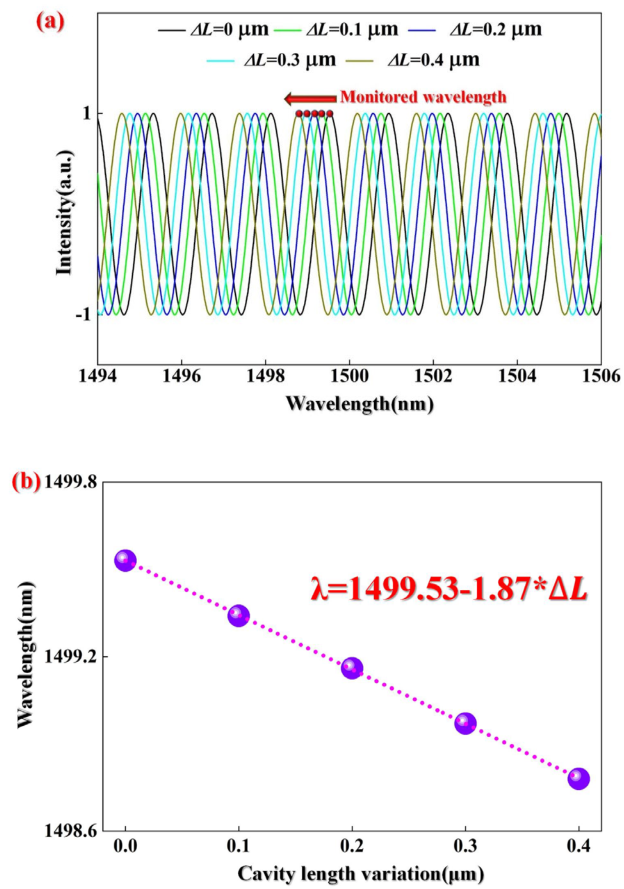

Fig.2. (a) Simulated sensing spectra as the cavity length decreases. (b) Wavelength response of the sensing interferometer.

Subsequently, the corresponding reference spectra can be generated based on equation (3). The central wavelength, λ_0, is determined to be 1500 nm and the corresponding reference spectra are shown in Fig. 3.

From Fig.3, the calculated reference spectra differ from the typical interferometric spectra, exhibiting a decrease in FSR as the wavelength increases. As the cavity length variation increases, the monitored wavelength shows a red shift, moving in the opposite direction to that of the sensing spectra. Ultimately, the output spectra can be obtained by superimposing the sensing spectra and the reference spectra. The output spectra generated based on the proposed scheme and their responses are shown in Fig. 4(a) and Fig. 4(b), which enhances the sensitivity by a factor of 22 times. The proposed approach enables a more compact sensing structure and resolves the issue of environmental disturbances affecting the reference interferometer, as will be further verified in the following experimental case.

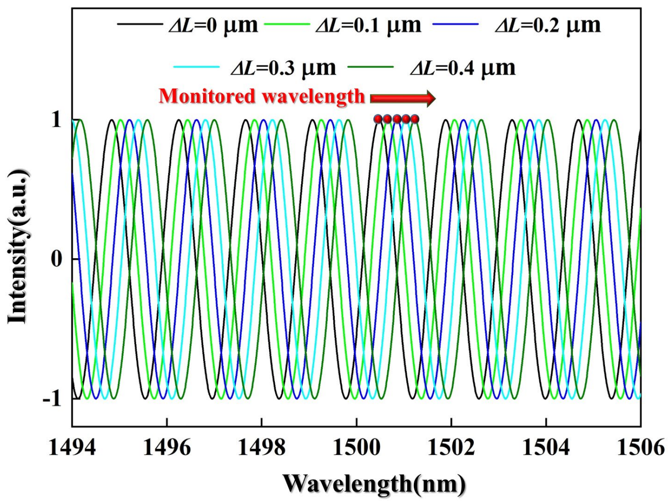

Fig.3. Calculated reference spectra correspond to the sensing spectra.

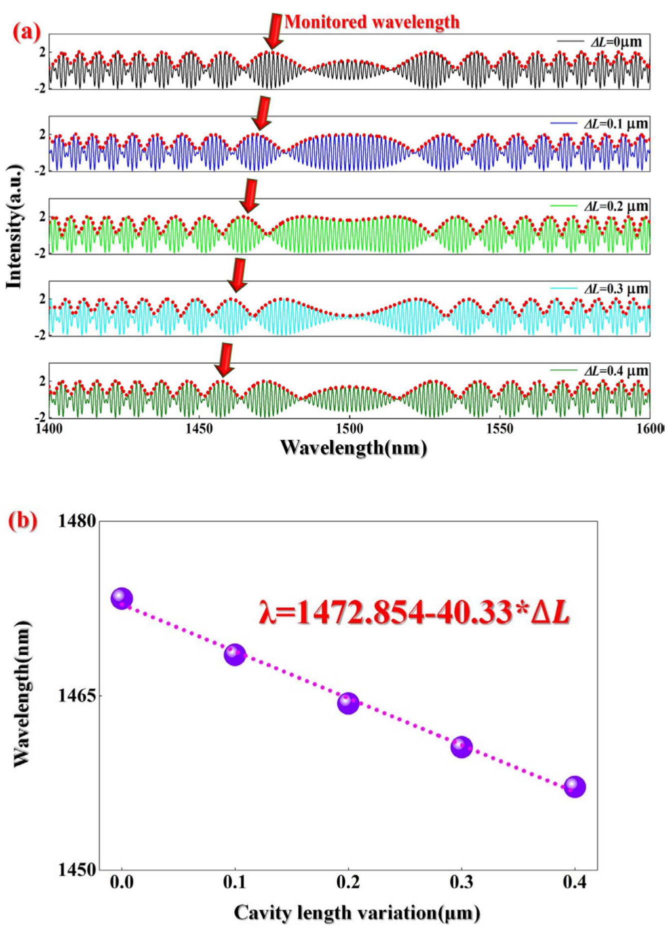

Fig.4. (a) Simulated output spectra as the cavity length decreases. (b) Wavelength responses of the output spectra.

III. Experimental Results And Discussion

A. Experimental Setup And The Performance Of The Sensing Interferometer

Environmental temperature is a fundamental physical parameter in daily life, serving as an example for measurement in this study. The corresponding experimental setup for temperature measurement is established, and the diagram is shown in Fig. 5. A broadband supercontinuum light source (BBS, YSL Co. Ltd.) with a wavelength range of 1500 nm to 1600 nm is employed. The light from the BBS is directed to the temperature FPI sensor under test. The transmitted light from the sensor is guided to an Optical Spectrum Analyzer (OSA, Yokogawa), where the sensing spectra can be obtained.

The FPI sensor is placed in a water bath and it is constructed by using two single-mode fibers encapsulated in commercial ceramic ferrules. The flat end faces of the fiber serve as the two reflectors of the interferometer, forming a Fabry-Perot cavity with water as the cavity medium. The two ceramic ferrules, made of alumina, are held in place by a matching alloy sleeve. As the alloy sleeve expands or contracts with temperature variations, the distance between the two ceramic ferrules changes, thereby altering the cavity length. This temperature sensor consists solely of optical fiber, ceramic ferrules, and an alloy sleeve, leveraging the high-temperature resistance and stability of these materials. The nested packaging and fixing method, using metal and ceramic components, ensures the sensor is waterproof and resistant to high temperatures, making it suitable for a wide range of applications.

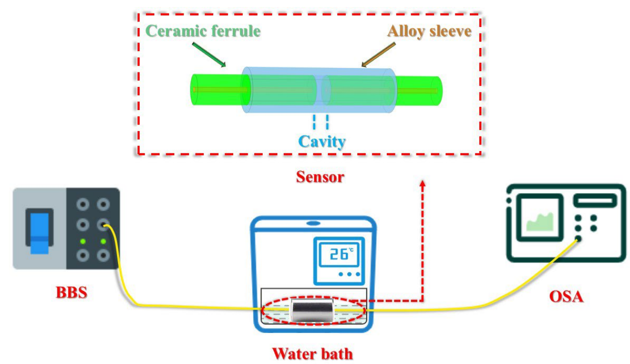

Fig. 5. Experimental setup for the temperature measurement.

The spectra of the sensing FPI, obtained from the OSA, are normalized as the temperature varies from 30.1 ℃ to 25.8 ℃, as shown in Fig. 6(a). It is evident that the dip wavelength near 1550 nm exhibits a blue shift as the temperature decreases. The corresponding temperature sensitivity is determined to be 0.148 nm/℃, as depicted in Fig. 6(b).

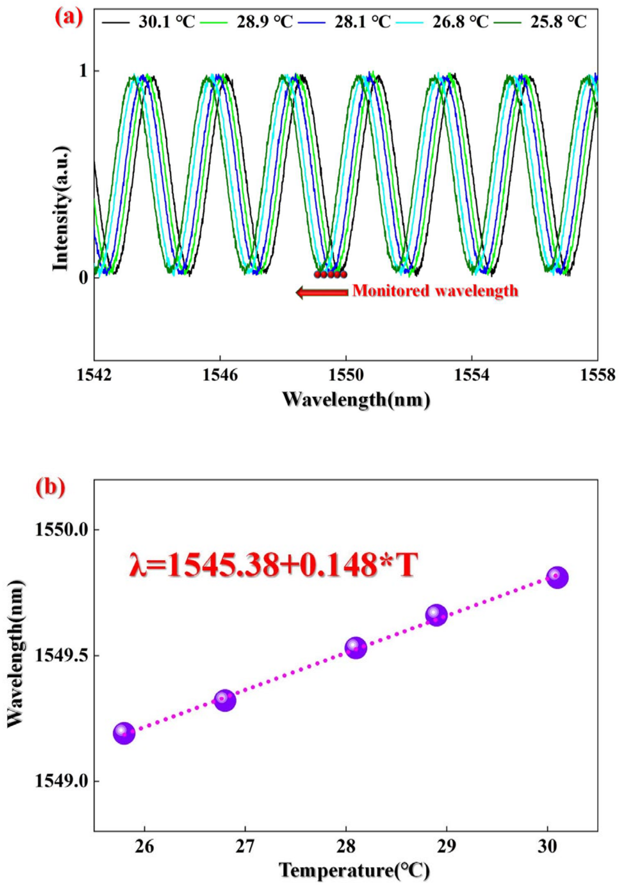

Fig. 6. Normalized spectra of the sensor as the temperature decreases from 30.1℃ to 25.8℃. (b) Wavelength response of the sensor with varying temperatures.

B. Performance Of The Conventional Vernier Effect Scheme

To improve the sensitivity, the conventional Vernier effect is applied by using a real reference FPI. The reference cell is paralleled with the sensing one through an optical coupler. Both the reference and sensing cells share the same structural design, and the reference cavity length can be adjusted manually to be close to the sensing cavity length. However, it is challenging to control the reference cavity length precisely, thereby limiting the size of the generated Vernier envelope and the performance of the sensitivity enhancement. To protect the reference cell from environmental disturbances, it is placed in a test chamber at a constant temperature, consistent with the initial temperature of the sensing cell. The corresponding experimental setup is shown in Fig.7.

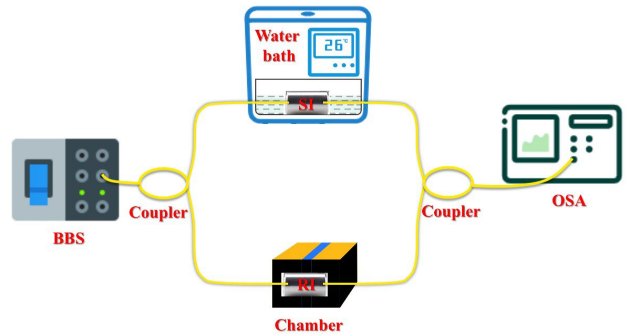

Fig.7. Experimental setup of the conventional Vernier effect scheme (SI: Sensing Interferometer, RI: Reference Interferometer).

Finally, the normalized superimposed spectra are measured and shown in Fig. 8(a) at different temperatures. The corresponding wavelength response is depicted in Fig. 8(b), indicating a temperature sensitivity of 0.607 nm/°C.

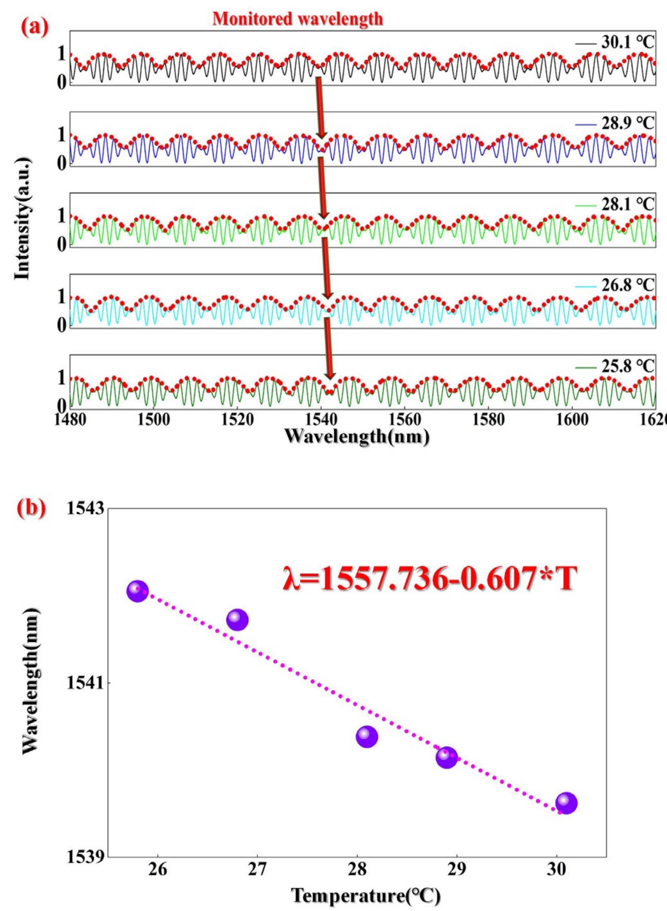

Fig. 8. (a) Normalized spectra of the conventional Vernier effect-based sensor as the temperature decreases from 30.1℃ to 25.8℃. (b) Wavelength response of the conventional Vernier effect-based sensor with varying temperatures.

C. Performance Of The Proposed Measurement Scheme

Finally, the proposed Vernier effect scheme is applied to compare its performance with that of the conventional Vernier effect. The inverted reference spectrum changes dynamically in response to variations in the sensing spectrum at different temperatures. Based on the sensing spectra measured in the previous section, the central wavelength, λ_0, is determined to be 1550 nm. Subsequently, the corresponding reference spectra can be calculated according to equation (3), as discussed in the theoretical section.

Then, by superimposing the calculated reference spectra and the measured sensing spectra, the resulting superimposed spectra are obtained and shown in Fig. 9(a) at different temperatures.

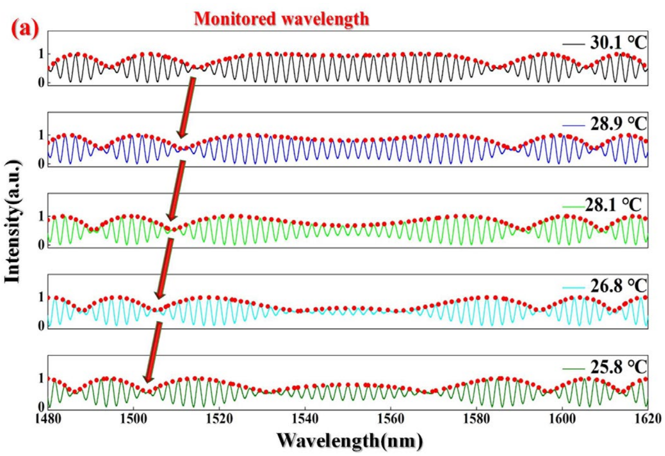

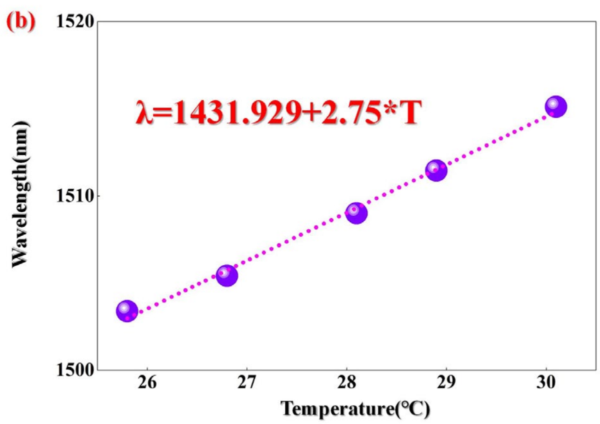

Fig. 9. (a) Normalized spectra of the proposed Vernier effect-based sensor as the temperature decreases from 30.1℃ to 25.8℃. (b) Wavelength response of the proposed Vernier effect-based sensor with varying temperatures.

According to the wavelength responses of the output spectra with varying temperatures depicted in Fig. 9(b), the corresponding temperature sensitivity is determined to be 2.75 nm/°C, which is nearly 19 times greater than that of the sensing interferometer. In comparison to the performance of the traditional Vernier effect-based sensor, the sensitivity achieved is nearly 5 times higher, only one interferometric sensor is involved in the configuration, and the need to stabilize the reference cell is eliminated, resulting in a simpler experimental setup and lower costs.

IV. Conclusions

In summary, this paper presents a novel Vernier effect scheme that eliminates the need for physically creating a reference interferometer through precision machining to match the FSR of the sensing interferometer. Instead, the reference interferometer spectrum is digitally constructed by inverting the sensing spectrum. This approach not only resolves the challenge of FSR matching between the two interferometers and improves the sensor's sensitivity, but also reduces the cost of the measurement system, offering considerable practical value. Additionally, the output spectrum of this variable-period Vernier effect features a highly identifiable unique wavelength, enabling long-term stable measurement by monitoring the wavelength changes of the peaks or dips near the unique wavelength. The proposed Vernier effect scheme opens new possibilities for cost-effective, high-performance sensing solutions in various applications.

Declaration of competing interest

Yunqing Guan has a related patent pending at Shenyang Ligong University. The authors declare that they have no known competing financial interests or personal relationships that could have appeared to influence the work reported in this paper.

References

[1] Y.X. Liu, X.G. Li, Y.N. Zhang, and Y. Zhao, "Fiber-optic sensors based on Vernier effect," *Measurement*, vol. 167, p. 108451, 2021.
[2] A.D. Gomes, H. Bartelt, and O. Frazao, "Optical Vernier effect: Recent advances and developments," *Laser Photon. Rev.*, vol. 15, p. 2000588, 2021.
[3] W. Naku, J. Huang and C. Zhu, "Optical fiber sensors based on advanced Vernier effect: A review," *IEEE Sensors J.*, vol. 24, no. 9, pp. 13758-13772, May 2024.
[4] T. Nan *et al.*, "Ultrasensitive strain sensor based on Vernier- effect improved parallel structured fiber-optic Fabry-Perot interferometer," *Opt. Exp.*, vol. 27, no. 12, pp. 17239-17250, 2019.
[5] P. Zhang *et al.*, "Cascaded fiber-optic Fabry-Perot interferometers with Vernier effect for highly sensitive measurement of axial strain and magnetic field," *Opt. Exp.*, vol. 22, no.16, pp. 19581-19588, 2014.
[6] X.P. Zhu *et al.*, "Ultra sensitive temperature sensor based on hybrid fiber optic interferometers and enhanced Vernier effect," *Optik*, vol. 294, p. 171455, Dec. 2023.
[7] Z.L. Xu, Y.Y. Luo, D.M. Liu, P.P. Shum and Q.Z. Sun, "Sensitivity-controllable refractive index sensor based on reflective θ-shaped microfiber resonator cooperated with Vernier effect," *Sci. Rep.*, vol. 7, no. 9620, Aug. 2017.
[8] R. Flores, R. Janeiro and J. Viegas, "Optical fibre Fabry-Pérot interferometer based on inline microcavities for salinity and temperature sensing," *Sci. Rep.*, vol. 9, no. 9556, July 2019.
[9] Y. Yang *et al.*, "Vernier Effect-Based Displacement Sensor Using In-Fiber Hollow Microsphere With a Hole," *IEEE Sensors J.*, vol. 23, no. 10, pp. 10509-10516, May 2023.
[10] H. Zhang *et al.*, "High-Sensitivity Transverse-Load and Axial-Strain Sensor Based on Air-Bubble Fabry–Pérot Cavity and Fiber Sagnac Loop Cascaded," *IEEE Sensors J.*, vol. 23, no. 6, pp. 5795-5802, March 2023.
[11] S.Y. Lin, F. Wang, Y.C. Qu, X.P. Han, Y.D. Zhang, "Discharge splicing-free ultra-highly sensitive fiber-optic temperature sensor based on PDMS and the Vernier effect," *Sens. Actuators A: Phys.*, vol. 376, p. 115653, Oct. 2024.
[12] H.F. Lin, F.F. Liu, H.Y. Guo, A. Zhou, and Y.T. Dai, "Ultra-highly sensitive gas pressure sensor based on dual side-hole fiber interferometers with Vernier effect," *Opt. Exp.*, vol. 26, no. 22, pp. 28763-28772, 2018.
[13] Z. Li *et al.*, "High-Sensitivity Gas Pressure Fabry–Perot Fiber Probe With Micro-Channel Based on Vernier Effect," *J. Lightw. Technol.*, vol. 37, no. 14, pp. 3444-3451, July 2019.

[14] X.M. Yang *et al.*, "Simplified highly-sensitive gas pressure sensor based on harmonic Vernier effect," *Opt. Laser Technol.*, vol. 140, p. 107007, Aug. 2021.

[15] A.D. Gomes *et al.*, "Hollow microsphere combined with optical harmonic Vernier effect for strain and temperature discrimination," *Opt. Laser Technol.*, vol. 127, p. 106198, July 2020.

[16] W.L. Yang *et al.*, "Highly sensitive fiber-optic temperature sensor with compact hybrid interferometers enhanced by the harmonic Vernier effect," *Opt. Exp.*, vol. 31, no. 9, pp. 14570-14582, 2023.

[17] A.D. Gomes *et al.*, "Optical harmonic Vernier effect: a new tool for high performance interferometric fiber sensors," *Sensors*, vol. 19, no. 24, p. 5431, 2019.

[18] A. Zornoza, J.A. Flores-Bravo, J. Zubia and J. Villatoro, "Sensitivity magnification of an interferometric optical fiber sensor with a length-linked virtual reference," *Opt. Laser Technol.*, vol. 167, p. 109819, Dec. 2023.

[19] Y.Q. Guan and X.P. Dong, "Sensitivity-enhanced flow rate sensor based on Vernier effect with a virtual reference cell," *IEEE Sensors J.*, vol. 22, no. 24, pp. 23915-23922, Dec. 2022.

[20] Y.Q. Guan and X.P. Dong, "Reconfigurable highly-sensitive interferometric sensor with Vernier effect and a virtually tunable reference cell," *Opt. Commun.,* vol. 535, May 2023.

[21] L. Liu *et al.*, "High-sensitivity strain sensor implemented by hybrid cascaded interferometers and the Vernier-effect," *Opt. Laser Technol.*, vol. 119, p. 105591, Nov. 2019.

[22] Y. Wang *et al.*, "Relative humidity sensor based on cascaded Fabry-Perot interferometers and Vernier effect," *Optik*, vol. 254, p. 168605, March 2022.

[23] S. Wang *et al.*, "In-situ adjustable fiber-optic piezometer based on parallelly structured external Fabry-Perot interferometers with Vernier effect and its harmonics," *Opt. Exp.*, vol. 29, no. 26, pp. 42800-42812, 2021.

[24] L. Chen, J. Li, F. Xie, J. Tian and Y. Yao, "High-Sensitivity Carcinoembryonic Antigen Detection Using Open Cavity Fabry-Perot Immunosensor Based on Vernier Effect," *J. Lightw. Technol.*, vol. 41, no. 13, pp. 4547-4554, July 2023.